Gait Generation of 22-DOF Humanoid Robot on Hard and Deformable Terrain with Double Support Phase

Sunil Gora[1], Shakti S Gupta[2] and Ashish Dutta[3]

***Abstract*— In real-world application, the humanoid robot may have to walk with each foot placed on terrains having different properties. The effect of terrain parameters can be included in the dynamics using the compliant contact model with a spring and a damper element. In this paper, the humanoid robot is modeled as a spherical inverted pendulum in the single support phase (SSP) and a suspended pendulum in the double support phase (DSP). In the DSP, a pendulum is assumed to be suspended at a virtual support point (VSP), and equivalent terrain parameters are used for contact modeling. The right and left leg foot of the humanoid robot are placed on terrains having different properties. The foot trajectories in the DSP are obtained by resolving forces using minimization of the moment about the VSP. The joint trajectories of the 22-DOF humanoid robot are optimized based on the motion of the simplified model such that the angular momentum about the center of mass (COM) is minimum. The simulation of the floating-base robot proves that the 22-DOF humanoid robot can walk on terrains with different properties by following the COM trajectory of the simplified model.**

I. INTRODUCTION

In traversing the real-world terrain, legged robots have improved significantly in the last few decades. The dynamic stability criterion of zero moment point [1] is used for walking on flat terrain [2], stairs [3] and inclined terrain [4]. For legged locomotion on uneven terrain, footstep planner and optimization-based walking stabilization and trajectory generation are used by Kuindersma et al. [5]. The kinematic constraints due to rigid foot-terrain contact assumption are an essential part of the controller design. Mesesan et al. [6] presented the stabilization of the stance foot by applying a damping wrench when the rigid contact assumption is violated. Xiong et al. [7] reduced the stability region by carrying out the experiment of static stability on granular terrain.

In the walking pattern generation, rigid contact is assumed for computational efficiency, however the robot may encounter terrains with different mechanical properties. The spring-damper model is used to include the effect of terrain properties in the dynamics of monopod hopper [8], nonlinear inverted pendulum [9] and 3D dual spring-loaded inverted pendulum [10]. The gait generation of a planer biped robot on inclined deformable terrain using the energy regions is presented in [11]. The terrain with different mechanical properties is used as unilateral perturbations to human gait [12]. However, the dynamically stable walking of robot on such terrain is not studied in the literature. In this paper, we present a method for locomotion of humanoid robot on terrains with different properties. The left and right leg foot of the humanoid robot are placed on deformable and hard terrain, respectively, as shown in Fig. 1. The humanoid robot is modeled as a spherical inverted pendulum in the SSP and a suspended pendulum in the DSP. In DSP, the pendulum is assumed to be suspended at a virtual support point (VSP) for smooth leg support transition, and equivalent terrain parameters are used for contact modeling. The salient contributions of the paper are as follows:

i Humanoid robot walking pattern generation in the DSP when each foot is placed on a different type of terrain, and

ii Gait generation of the humanoid robot using spherical inverted pendulum motion with minimized angular momentum about the COM.

The rest of the paper is organized as follows: In Section II, the dynamics of a humanoid robot and simplified dynamics as a spherical inverted pendulum are presented. The double support phase model is shown in Section III. The minimum angular momentum formulation is presented in Section IV. In

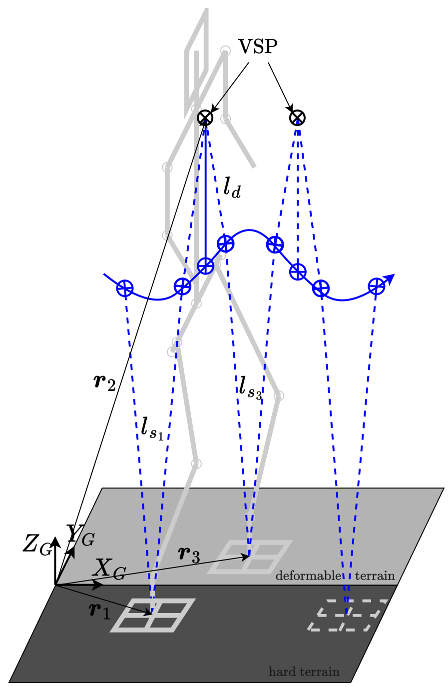

Fig. 1: Walking pattern of COM in DSP when both feet of the robot are placed on different types of terrains

*All Authors are with the Department of Mechanical Engineering, Indian Institute of Technology Kanpur, India. Email: [1] sunilg@iitk.ac.in, [2]ssgupta@iitk.ac.in, [3]adutta@iitk.ac.in

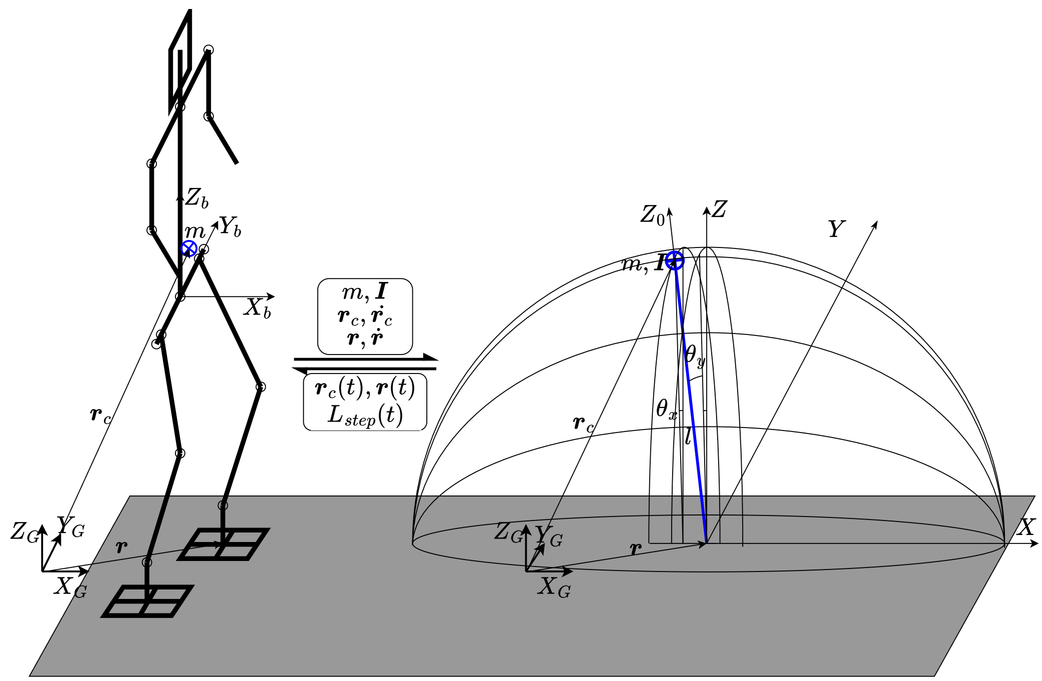

Fig. 2: 22-DOF humanoid robot (left) and spherical inverted pendulum model (right)

Section V, the simulation trajectories and the variation from the desired trajectories are analyzed. Finally, conclusions and the scope of future work are presented in Section VI.

II. Dynamic Modeling of Humanoid Robot

A. 22-DOF humanoid robot

In Fig. 2, a humanoid robot and simplified dynamics as a spherical inverted pendulum model are shown. The humanoid robot has 22 degrees of freedom: 6 in each leg, 3 in the torso, 3 in each hand, and 1 in the head. The floating-base representation is used in dynamic modeling, and the floating-base is attached to the center of the hip link. The position and orientation of the floating-base are represented by virtual joint coordinates, which are denoted by $\boldsymbol{q}_0 \in \mathbb{R}^{6\times1}$. The active joint coordinates are denoted by $\boldsymbol{q}_\theta \in \mathbb{R}^{22\times1}$. The dynamics of the robot [13] can be expressed as

$$\begin{bmatrix} \boldsymbol{I}_0 & \boldsymbol{I}_{0\theta} \\ \boldsymbol{I}_{0\theta}^T & \boldsymbol{I}_\theta \end{bmatrix} \begin{bmatrix} \ddot{\boldsymbol{q}}_0 \\ \ddot{\boldsymbol{q}}_\theta \end{bmatrix} + \begin{bmatrix} \boldsymbol{c}_0 \\ \boldsymbol{c}_\theta \end{bmatrix} = \begin{bmatrix} \boldsymbol{0} \\ \boldsymbol{\tau}_\theta \end{bmatrix} + \sum_{i=1}^{e_n} \begin{bmatrix} \boldsymbol{J}_{i_0}^T \\ \boldsymbol{J}_{i_\theta}^T \end{bmatrix} \boldsymbol{w}_i. \tag{1}$$

Here, $\boldsymbol{I}_0 \in \mathbb{R}^{6\times6}$ and $\boldsymbol{I}_\theta \in \mathbb{R}^{22\times22}$ are the inertia matrices of the base and links, respectively, $\boldsymbol{I}_{0\theta} \in \mathbb{R}^{6\times22}$ is the coupling inertia matrix, $\boldsymbol{c}_0 \in \mathbb{R}^{6\times1}$ and $\boldsymbol{c}_\theta \in \mathbb{R}^{22\times1}$ are the vectors of position and velocity dependent terms associated with the base and links, respectively, $\boldsymbol{\tau}_\theta \in \mathbb{R}^{22\times1}$ is the joint torques vector, $\boldsymbol{J}_{i_0} \in \mathbb{R}^{6\times6}$ and $\boldsymbol{J}_{i_\theta} \in \mathbb{R}^{6\times22}$ are the Jacobian matrices which map the joint coordinates of the base and links, respectively to the angular and linear velocity of i^{th} contact point, $\boldsymbol{w}_i \in \mathbb{R}^{6\times1}$ is the wrench vector acting at i^{th} contact point and e_n is the number of points where the contact force is acting on the robot.

B. Spherical Inverted Pendulum

The robot dynamics in the SSP is simplified as a spherical inverted pendulum (SIP) model of mass m and length l, which is shown in Fig. 2. The position of the COM of the SIP $\boldsymbol{r}_c = [x_c, y_c, z_c]^T$ in terms of the position of the contact point $\boldsymbol{r} = [x, y, z]^T$ can be written as

$$\boldsymbol{r}_c = \boldsymbol{r} + \boldsymbol{R}_{\theta_x}\boldsymbol{R}_{\theta_y}\begin{bmatrix}0, & 0, & l\end{bmatrix}^T. \tag{2}$$

Here, $\boldsymbol{R}_{\theta_x}$ and $\boldsymbol{R}_{\theta_y}$ are rotation matrices for the frame rotation about the current x and y axis, respectively. The Euler angles of rotation are θ_x and θ_y. The generalized joint coordinates of the pendulum are given as

$$\boldsymbol{q}_p = \begin{bmatrix}\boldsymbol{r}^T & \theta_x & \theta_y\end{bmatrix}^T. \tag{3}$$

The equations of motion of the pendulum are written as

$$\boldsymbol{I}_p\ddot{\boldsymbol{q}}_p + \boldsymbol{c}_p = \boldsymbol{J}_p^T\boldsymbol{f}_p. \tag{4}$$

Here, $\boldsymbol{I}_p \in \mathbb{R}^{5\times5}$ is the inertia matrix, $\boldsymbol{c}_p \in \mathbb{R}^{5\times1}$ is the vector of the centrifugal, Coriolis and gravitational forces, $\boldsymbol{J}_p \in \mathbb{R}^{3\times5}$ is the Jacobian matrix and $\boldsymbol{f}_p \in \mathbb{R}^{3\times1}$ is the vector of the contact forces. The contact force vector $\boldsymbol{f}_p =$

$[\boldsymbol{f}_t^T, f_n]^T$ is obtained using the spring-damper contact model [9]. The normal contact force f_n is written as

$$f_n = \begin{cases} -k_n\delta_n - c_n\dot{\delta}_n, & \delta_n < 0 \ \& \ \dot{\delta}_n < 0, \\ -k_n\delta_n, & \delta_n < 0 \ \& \ \dot{\delta}_n \geq 0, \\ 0, & \delta_n \geq 0, \end{cases} \tag{5}$$

where δ_n and $\dot{\delta}_n$ are the contact point's displacement and relative velocity with respect to the terrain in the normal direction, k_n and c_n are the stiffness and damping parameters of the terrain, respectively. The contact point's relative position and velocity vector in the tangential plane are $\boldsymbol{\delta}_t$ and $\dot{\boldsymbol{\delta}}_t$. The tangential force vector $\boldsymbol{f}_t$ is given by

$$\boldsymbol{f}_t = \begin{cases} -k_t\boldsymbol{\delta}_t - c_t\dot{\boldsymbol{\delta}}_t, & \|\boldsymbol{f}_t\| < \mu f_n, \\ \frac{\mu f_n}{\|-k_t\boldsymbol{\delta}_t - c_t\dot{\boldsymbol{\delta}}_t\|}(-k_t\boldsymbol{\delta}_t - c_t\dot{\boldsymbol{\delta}}_t), & \|\boldsymbol{f}_t\| \geq \mu f_n, \end{cases} \tag{6}$$

where k_t and c_t are the stiffness and damping parameters in the tangential direction, and μ is the coefficient of friction and assumed to be sufficiently high for the No-slip condition. Also, for flat terrain, the Z_G axis is in the normal direction, and the XY plane is the tangential plane. In this case, the normal force is $f_n = f_z$, and the tangential force vector is $\boldsymbol{f}_t = [f_x, f_y]^T$.

III. Double support phase

The DSP is modeled assuming the COM is suspended from a point called virtual support point (VSP) [14] as shown in Fig. 1. The position vector of the VSP (derivation is shown in the Appendix) is obtained as

$$\boldsymbol{r}_2 = \boldsymbol{r}_c - (\boldsymbol{r}_1 + \Delta\boldsymbol{r} - \boldsymbol{r}_c)p_d, \tag{7}$$

where,

$$p_d = \frac{l_d}{\|\boldsymbol{r}_1 + \Delta\boldsymbol{r} - \boldsymbol{r}_c\|}, \tag{8}$$

$$\Delta\boldsymbol{r} = \begin{bmatrix} \frac{\dot{y}_c L_z}{m(\dot{x}_c^2+\dot{y}_c^2)} \\ -\frac{\dot{x}_c L_z}{m(\dot{x}_c^2+\dot{y}_c^2)} \\ 0 \end{bmatrix}. \tag{9}$$

Here, L_z is the angular momentum of the SIP in the Z_G direction about the contact point.

A. Effect of different terrain stiffness on SIP

The periodic trajectory of the SIP with DSP has no continuous energy input, and the energy loss due to impact is also negligible. In DSP, both feet are placed on terrains with different stiffness. The energy-efficient periodic trajectory requires different pendulum lengths of consecutive SIP models depending on the difference in terrain stiffness. Let the foot-terrain contact stiffness in the normal direction for both feet are denoted by k_{n_1} and k_{n_3}, respectively. The difference in the pendulum lengths can be written as

$$l_{s_3} - l_{s_1} = \frac{k_{n_1} - k_{n_3}}{mg}. \tag{10}$$

The kinematic constraint for walking with this condition is that the difference between the current height (z_e) and the full extended height (z_{ext}) at $x_{ext} = x_e$ of the swing leg foot must be greater than the difference in the pendulum lengths, i.e.,

$$|z_{ext} - z_e| > |\frac{k_{n_1} - k_{n_3}}{mg}|. \tag{11}$$

B. Leg trajectories during DSP

Let the contact force obtained during the DSP is $\boldsymbol{f}_2 = [\boldsymbol{f}_{t_2}^T, f_{n_2}]^T$, which is the resultant of $\boldsymbol{f}_1$ and $\boldsymbol{f}_3$ acting on both feet simultaneously. Here, the equivalent normal terrain stiffness in the DSP is

$$k_{n_2} = k_{n_1} + k_{n_3}. \tag{12}$$

The relative position of the contact point in the normal and tangential direction is denoted δ_{n_2} and $\boldsymbol{\delta}_{t_2}$, respectively. The foot-terrain contact stiffness for both feet in the tangential direction are denoted by k_{t_1} and k_{t_3}. By considering the foot's velocity and acceleration negligible, the contact force and the relative position of the contact point relation is written as

$$\boldsymbol{f}_i = \boldsymbol{k}_i \odot \boldsymbol{\delta}_i, \tag{13}$$

where, $\boldsymbol{k}_i = [k_{t_i}, k_{t_i}, k_{n_i}]^T$ is the vector of tangential and normal stiffness, and $\odot$ denotes the element-wise multiplication of two vectors. The relative change in the positions of both contact leg feet $\boldsymbol{\delta}_i = [\boldsymbol{\delta}_{t_i}^T, \delta_{n_i}]^T$ are determined by minimizing the moment of the forces $\boldsymbol{f}_1$ and $\boldsymbol{f}_3$ as

$$\begin{aligned} \min_{\boldsymbol{\delta}_i} \quad & || \sum_{i=1,3} (\boldsymbol{r}_i + \boldsymbol{\delta}_i - \boldsymbol{r}_2) \times (\boldsymbol{k}_i \odot \boldsymbol{\delta}_i)||, \\ \text{s.t.} \quad & k_{t_i}\|\boldsymbol{\delta}_{t_i}\| \leq \mu k_{ni}\delta_{n_i}, \ i = 1,3 \ , \\ & k_{t_1}\boldsymbol{\delta}_{t_1} + k_{t_3}\boldsymbol{\delta}_{t_3} = k_{t_2}\boldsymbol{\delta}_{t_2}, \\ & k_{n_1}\delta_{n_1} + k_{n_3}\delta_{n_3} = k_{n_2}\delta_{n_2}. \end{aligned} \tag{14}$$

IV. Minimization of angular momentum

The primary task of the humanoid robot is to follow the COM and leg trajectories without any change in the hip orientation. The desired trajectories are arranged in the form of linear equation as

$$\boldsymbol{J}_1\dot{\boldsymbol{q}} = \boldsymbol{t}_1. \tag{15}$$

Here, the matrices $\boldsymbol{J}_1 \in \mathbb{R}^{18\times28}$ and $\boldsymbol{t}_1 \in \mathbb{R}^{18\times28}$ are written as

$$\boldsymbol{J}_1 = \begin{bmatrix}\boldsymbol{J}_{v_c}^T, & \boldsymbol{J}_{\omega_0}^T, & \boldsymbol{J}_{v_e}^T, & \boldsymbol{J}_{\omega_e}^T\end{bmatrix}^T, \tag{16}$$

$$\boldsymbol{t}_1 = \begin{bmatrix}\boldsymbol{v}_c^T, & \boldsymbol{\omega}_0^T, & \boldsymbol{v}_e^T, & \boldsymbol{\omega}_e^T\end{bmatrix}^T, \tag{17}$$

where, $\boldsymbol{J}_{v_c} \in \mathbb{R}^{3\times28}$ is the Jacobian matrix, which maps the rate of joint coordinates to the linear velocity of the COM [15], $\boldsymbol{J}_{\omega_0} \in \mathbb{R}^{3\times28}$ is the Jacobian matrix, which maps the joint rates to the angular velocity of the floating-base, $\boldsymbol{J}_{v_e} \in \mathbb{R}^{6\times28}$ and $\boldsymbol{J}_{\omega_e} \in \mathbb{R}^{6\times28}$ are the Jacobian matrices, which map the joint rates to the linear and angular velocities of both leg ankles, respectively. $\boldsymbol{v}_c$ is the velocity vector of the COM, and $\boldsymbol{\omega}_0$ is the angular velocity vector of the floating-base. $\boldsymbol{v}_e$ and $\boldsymbol{\omega}_e$ are the linear and angular velocity vectors of both leg ankles, respectively. The minimum norm solution for joint rates [16] is written as

$$\dot{\boldsymbol{q}}_1 = \boldsymbol{J}_1^+\boldsymbol{t}_1. \tag{18}$$

Here, $\boldsymbol{J}_1^+$ is the Moore–Penrose inverse of the matrix $\boldsymbol{J}_1$.

A. Angular momentum

The motion of the robot obtained from Eq. (18) generates angular momentum about the COM, which was considered negligible in the simplified dynamics. The minimization of the angular momentum about the COM results in the minimal change of the actual center of pressure (COP) from the desired. The COP at the center of the foot also ensures no rotation of the foot on deformable terrain. The secondary task of the humanoid robot is angular momentum minimization, which is expressed as

$$\boldsymbol{J}_2\dot{\boldsymbol{q}} = \boldsymbol{t}_2, \tag{19}$$

where,

$$\boldsymbol{J}_2 = \boldsymbol{I}_c\boldsymbol{J}_{\omega_c}, \tag{20}$$

$$\boldsymbol{t}_2 = \boldsymbol{0}. \tag{21}$$

Here, $\boldsymbol{I}_c \in \mathbb{R}^{3\times3}$ is the rigid body inertia matrix about the COM and $\boldsymbol{J}_{\omega_c} \in \mathbb{R}^{3\times28}$ is the Jacobian matrix, which maps the joint rates to the angular velocity of the robot and $\boldsymbol{0}^{3\times1}$ is the zero vector. The next solution for joint rates is obtained as

$$\dot{\boldsymbol{q}}_2 = \dot{\boldsymbol{q}}_1 + \tilde{\boldsymbol{J}}_2^{+}(\boldsymbol{t}_2 - \boldsymbol{J}_2\dot{\boldsymbol{q}}_1), \tag{22}$$

where,

$$\tilde{\boldsymbol{J}}_2 = \boldsymbol{J}_2\boldsymbol{P}_1, \tag{23}$$

$$\boldsymbol{P}_1 = \boldsymbol{E} - \boldsymbol{J}_1^{+}\boldsymbol{J}_1. \tag{24}$$

Here, $\boldsymbol{E} \in \mathbb{R}^{28\times28}$ is the identity matrix, and $\boldsymbol{P}_1$ is a projector into the null space of $\boldsymbol{J}_1$. The arms of the humanoid robot have redundancy, which can be utilized further to minimize the robot's kinetic energy. The minimization problem is formulated as

$$\min_{\dot{\boldsymbol{\zeta}}} \quad \frac{1}{2}(\dot{\boldsymbol{q}}_2 + \boldsymbol{P}_2\dot{\boldsymbol{\zeta}})^T\boldsymbol{I}(\dot{\boldsymbol{q}}_2 + \boldsymbol{P}_2\dot{\boldsymbol{\zeta}}), \tag{25}$$

where,

$$\boldsymbol{P}_2 = \boldsymbol{P}_1 - \tilde{\boldsymbol{J}}_2^{+}\tilde{\boldsymbol{J}}_2, \tag{26}$$

$$\boldsymbol{I} = \begin{bmatrix} \boldsymbol{I}_0 & \boldsymbol{I}_{0\theta} \\ \boldsymbol{I}_{0\theta}^T & \boldsymbol{I}_\theta \end{bmatrix}. \tag{27}$$

Here, $\dot{\boldsymbol{\zeta}} \in \mathbb{R}^{28\times1}$ is the vector that optimizes the joint rates using the null space projection matrix $\boldsymbol{P}_2$. The constraints are the maximum joint rates and joint angle limits of the motors. The constrained optimization problem is solved using MATLAB's inbuilt function '*fmincon*'. The final solution for the joint rates is obtained as

$$\dot{\boldsymbol{q}}_3 = \dot{\boldsymbol{q}}_2 + \boldsymbol{P}_2\dot{\boldsymbol{\zeta}}. \tag{28}$$

V. Results

The parameters of the 22-DOF humanoid robot [17] for simulation are listed in Table I. The normal terrain stiffness parameters are shown in the table, which are assumed to be the same in tangential direction for simplicity [18]. The normal terrain stiffness of deformable terrain is obtained using a polyurethane foam sheet of density $16\,\mathrm{kg/m^3}$, which is deformed under the self-weight of the robot. The left leg foot of the robot is placed on deformable terrain, whereas the right leg foot is on hard terrain. The simplified dynamics model generates the COM motion, contact leg trajectories and step length for periodic walking. The step length and maximum height from the ground are used in the cubic spline trajectory of the swing leg foot. The joint angle trajectories are obtained by integration of joint rates given in Eq. (28), which are plotted in Fig. 3. In inverse dynamics of the humanoid robot, the floating-base accelerations are obtained and integrated for the time interval of 1.5 seconds. The snapshots of the humanoid robot walking two steps forward are shown in Fig. 4. The desired and simulated motion of the COM is shown in Fig. 5. The deviation of the COM trajectory is negligible, which is evident in the figure. The angular momentum of the robot about the COM is plotted in Fig. 6, which is shown to be negligible during walking. The angular momentum of the hip, legs, torso, head and arms are

TABLE I: Humanoid robot simulation parameters

Mass of robot (m)	$1.375\,\mathrm{kg}$
Mass of hip-link	$0.151\,\mathrm{kg}$
Mass of each leg	$0.264\,\mathrm{kg}$
Mass of each hand	$0.124\,\mathrm{kg}$
Mass of torso and head	$0.447\,\mathrm{kg}$
Thigh length	$65\,\mathrm{mm}$
Shank length	$65\,\mathrm{mm}$
Ankle height from foot	$26\,\mathrm{mm}$
Maximum joint rates	$8\,\mathrm{rad/s}$
Foot size	$78\,\mathrm{mm} \times 122\,\mathrm{mm}$
Normal stiffness of hard terrain	$49\,564.9\,\mathrm{N/m}$
Normal stiffness of deformable terrain	$2248.125\,\mathrm{N/m}$
Damping ratio (ζ)	0.3
Coefficient of friction (μ)	0.5
Initial position of COM (in m)	$(-0.0036, 0.0176, 0.1977)$
Initial position of hip-link center (in m)	(0, 0.0323, 0.2188)
Initial velocity of hip-link center (in m/s)	(0.05, 0.05, 0)

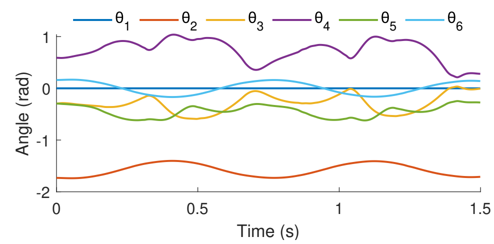

(a) Joint positions of left leg

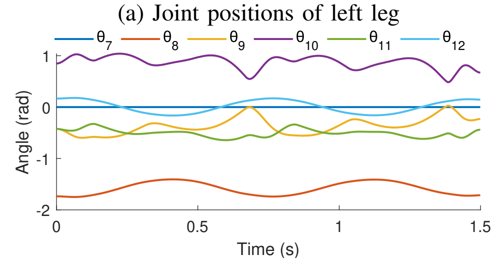

(b) Joint positions of right leg

Fig. 3: Leg joint trajectories for walking on hard (left foot) and deformable (right foot) terrain

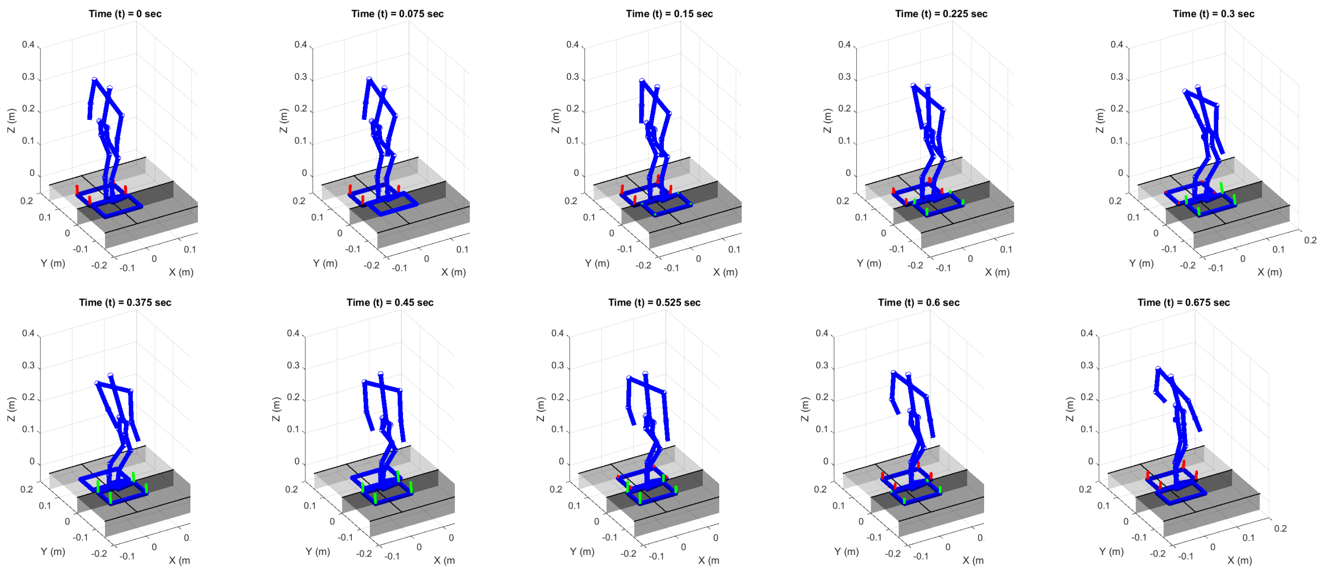

Fig. 4: Humanoid robot walking two steps forward on hard (right foot) and deformable (left foot) terrain

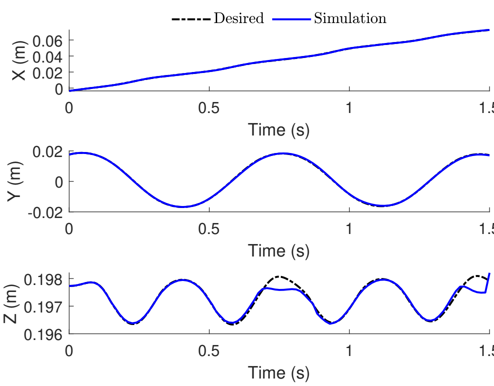

Fig. 5: Desired and simulation trajectory of the COM

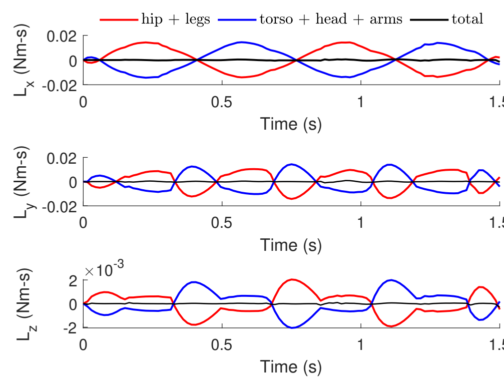

Fig. 6: Angular momentum of the robot about the COM

also shown in the figure. The COP obtained from the normal contact forces on both feet and COM motion are shown in Fig. 7. The COP is maintained close to the center of the foot in the SSP, and the transition of the COP is continuous in the DSP, which is evident from the plot. The desired orientation of the floating-base hip is fixed at the initial pose, and the error in the hip orientation angle due to foot rotation is shown in Fig. 8.

VI. CONCLUSIONS

In this paper, 22-DOF humanoid robot is modeled as a spherical inverted pendulum in the single support phase and a suspended pendulum in the double support phase. The leg support transition in the double support phase when each foot is placed on terrain of different mechanical properties is presented. The leg motions during the double support phase are obtained by using the terrain stiffness with forces and moments resolution. The joint motions with minimum angular momentum are generated, and the variation in the desired and simulation trajectories are analyzed. The center

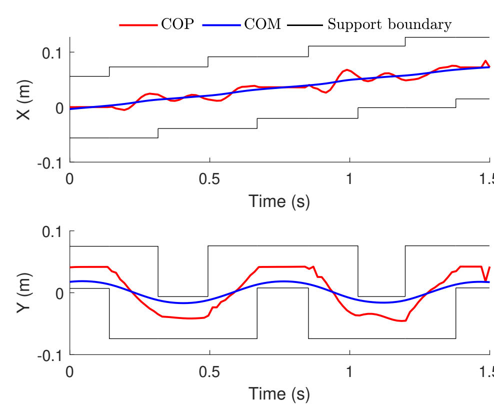

Fig. 7: COP and COM over the period of walking

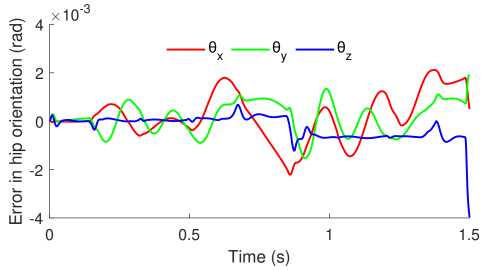

Fig. 8: Error in the desired orientation of the hip link

of pressure and error in the desired hip orientation obtained using floating-base dynamics are also analyzed. The simulation results show that the robot can walk on terrains with different properties. In future work, the walking of humanoid robot on uneven deformable terrain will be explored with experimental validation.

APPENDIX

The mass moment of inertia of the spherical pendulum about the COM is considered small to minimize the angular momentum about the COM [9]. The angular momentum of the spherical pendulum in the SSP about the contact point in the Z_G direction is constant, i.e.

$$(x_c - x_1)\dot{y}_c - (y_c - y_1)\dot{x}_c = \frac{L_z}{m}. \tag{29}$$

The suspended pendulum in DSP is a special case of the SIP when the motion is in a single plane. The angular momentum in the Z_G direction of the suspended pendulum about VSP is zero, i.e.,

$$(x_c - x_2)\dot{y}_c - (y_c - y_2)\dot{x}_c = 0. \tag{30}$$

Let the position of the center of pressure at the start of DSP with respect to $\boldsymbol{r}_1$ is $\Delta\boldsymbol{r}$, which is the intersection of the line passing from the COM and VSP with the terrain. For a minimum change of position of the COP, the distance between the COP at the end of SSP and the COP at the start of DSP should be minimum. Hence, the position vector $(\Delta x, \Delta y)$ is perpendicular to the velocity of the COM $(\dot{x}_c, \dot{y}_c)$ in the transverse plane, i.e.,

$$\dot{x}_c\Delta x + \dot{y}_c\Delta y = 0. \tag{31}$$

Also, using Eq. (29), the relation between the position vector, $(\Delta x, \Delta y)$ and L_z can be written as

$$\dot{y}_c\Delta x - \dot{x}_c\Delta y = \frac{L_z}{m}. \tag{32}$$

By solving Eqs. (31) and (32), we get

$$\Delta x = \frac{\dot{y}_c L_z}{m(\dot{x}_c^2 + \dot{y}_c^2)}, \tag{33}$$

$$\Delta y = -\frac{\dot{x}_c L_z}{m(\dot{x}_c^2 + \dot{y}_c^2)}. \tag{34}$$

Considering the robot foot flat, the intersection point of the line passing from the COM and VSP with the foot support area is at $z = z_1$, i.e., $\Delta z = 0$. Using the length of the suspended pendulum in DSP l_d, the position of the VSP is obtained as in Eq. 7. The foot placement position vector $\boldsymbol{r}_3$ is obtained as

$$x_3 = x_1 + 2(x_2 - x_1), \tag{35}$$

$$y_3 = y_1 + 2(y_2 - y_1), \tag{36}$$

$$z_3 = z_1 + mg\Big(\frac{k_{n_3} - k_{n_1}}{k_{n_1}k_{n_3}}\Big). \tag{37}$$

REFERENCES

[1] M. Vukobratović and B. Borovac, "Zero-moment point—thirty five years of its life," *International journal of humanoid robotics*, vol. 1, no. 01, pp. 157–173, 2004.

[2] A. Sarkar and A. Dutta, "8-dof biped robot with compliant-links," *Robotics and Autonomous Systems*, vol. 63, pp. 57–67, 2015.

[3] T. Sato, S. Sakaino, E. Ohashi, and K. Ohnishi, "Walking trajectory planning on stairs using virtual slope for biped robots," *IEEE transactions on industrial electronics*, vol. 58, no. 4, pp. 1385–1396, 2010.

[4] A. Sarkar and A. Dutta, "Optimal trajectory generation and design of an 8-dof compliant biped robot for walk on inclined ground," *Journal of Intelligent & Robotic Systems*, vol. 94, no. 3, pp. 583–602, 2019.

[5] S. Kuindersma, R. Deits, M. Fallon, A. Valenzuela, H. Dai, F. Permenter, T. Koolen, P. Marion, and R. Tedrake, "Optimization-based locomotion planning, estimation, and control design for the atlas humanoid robot," *Autonomous robots*, vol. 40, no. 3, pp. 429–455, 2016.

[6] G. Mesesan, J. Englsberger, G. Garofalo, C. Ott, and A. Albu-Schäffer, "Dynamic walking on compliant and uneven terrain using dcm and passivity-based whole-body control," in *2019 IEEE-RAS 19th International Conference on Humanoid Robots (Humanoids)*. IEEE, 2019, pp. 25–32.

[7] X. Xiong, A. D. Ames, and D. I. Goldman, "A stability region criterion for flat-footed bipedal walking on deformable granular terrain," in *2017 IEEE/RSJ International Conference on Intelligent Robots and Systems (IROS)*. IEEE, 2017, pp. 4552–4559.

[8] V. Vasilopoulos, I. S. Paraskevas, and E. G. Papadopoulos, "Compliant terrain legged locomotion using a viscoplastic approach," in *2014 IEEE/RSJ International Conference on Intelligent Robots and Systems*. IEEE, 2014, pp. 4849–4854.

[9] S. Gora, S. S. Gupta, and A. Dutta, "Energy-based footstep planning of biped on uneven deformable terrain using nonlinear inverted pendulum," *Journal of Mechanisms and Robotics*, vol. 15, no. 5, 2023.

[10] C. Karakasis, I. Poulakakis, and P. Artemiadis, "An energy-based framework for robust dynamic bipedal walking over compliant terrain," *Journal of Dynamic Systems, Measurement, and Control*, vol. 146, no. 2, p. 021008, 2024.

[11] S. Gora, S. S. Gupta, and A. Dutta, "Gait generation of 6-dof biped robot on inclined deformable terrain using nonlinear inverted pendulum," in *Proceedings of the 2023 6th International Conference on Advances in Robotics*, 2023, pp. 1–6.

[12] V. Chambers and P. Artemiadis, "A model-based analysis of the effect of repeated unilateral low stiffness perturbations on human gait: Toward robot-assisted rehabilitation," in *2023 IEEE International Conference on Robotics and Automation (ICRA)*. IEEE, 2023, pp. 12 631–12 637.

[13] S. Gora, S. S. Gupta, and A. Dutta, "Optimal gait generation of an 8-dof biped robot on deformable terrain using floating-base dynamics," in *Advances in Robotics-5th International Conference of The Robotics Society*, 2021, pp. 1–6.

[14] M. Shibuya, T. Suzuki, and K. Ohnishi, "Trajectory planning of biped robot using linear pendulum mode for double support phase," in *IECON 2006-32nd Annual Conference on IEEE Industrial Electronics*. IEEE, 2006, pp. 4094–4099.

[15] T. Sugihara and Y. Nakamura, "Whole-body cooperative balancing of humanoid robot using cog jacobian," in *IEEE/RSJ international conference on intelligent robots and systems*, vol. 3. IEEE, 2002, pp. 2575–2580.

[16] T. Yoshikawa, *Foundations of robotics: analysis and control*. MIT press, 1990.

[17] "Kondo KHR-3HV humanoid robot," https://kondo-robot.com/, accessed: Nov. 01, 2023.

[18] T. W. Lambe and R. V. Whitman, *Soil mechanics*. John Wiley & Sons, 1991, vol. 10.